ELSEVIER

Identification of potent inhibitors of arenavirus and SARS-CoV-2 exoribonucleases by fluorescence polarization assay

Sergio Hernández [a], Mikael Feracci [a], Carolina Trajano De Jesus [a], Priscila El Kazzi [a], Rafik Kaci [a], Laura Garlatti [a], Clemence Mondielli [b], Fabrice Bailly [c], Philippe Cotelle [c,d], Franck Touret [e], Xavier de Lamballerie [e], Bruno Coutard [e], Etienne Decroly [a], Bruno Canard [a], François Ferron [a,**], Karine Alvarez [a,*]

[a] Université Aix-Marseille, Architecture et Fonction des Macromolécules Biologiques (AFMB) – UMR7257 CNRS – Case 932, 163 avenue de Luminy, Marseille CEDEX 09, 13288, France
[b] Evotec (France) SAS, Campus Curie, 195 route d'Espagne, 31036, Toulouse CEDEX, France
[c] Univ Lille, INSERM, CHU Lille, UMR-S 1172, Lille Neuroscience and Cognition Research Center, F-59000, Lille, France
[d] ENSCL-Centrale Lille, CS 90108, F-59652, Villeneuve d'Ascq, France
[e] Unité des Virus Émergents (UVE: Aix-Marseille University -IRD 190-Inserm 1207-IHU Méditerranée Infection), Marseille, France

ARTICLE INFO

ABSTRACT

Viral exoribonucleases are uncommon in the world of RNA viruses. To date, they have only been identified in the *Arenaviridae* and the *Coronaviridae* families. The exoribonucleases of these viruses play a crucial role in the pathogenicity and interplay with host innate immune response. Moreover, coronaviruses exoribonuclease is also involved in a proofreading mechanism ensuring the genetic stability of the viral genome. Because of their key roles in virus life cycle, they constitute attractive target for drug design.

Here we developed a sensitive, robust and reliable fluorescence polarization assay to measure the exoribonuclease activity and its inhibition *in vitro*. The effectiveness of the method was validated on three different viral exoribonucleases, including SARS-CoV-2, Lymphocytic Choriomeningitis and Machupo viruses. We performed a screening of a focused library consisting of 113 metal chelators. Hit compounds were recovered with an IC$_{50}$ at micromolar level. We confirmed 3 hits in SARS-CoV-2 infected Vero-E6 cells.

1. Introduction

Arenaviruses are emerging RNA viruses associated with fatal neurological and hemorrhagic diseases in humans. Currently there is only ribavirin as FDA-approved antiviral. For coronaviruses, in the context of the global SARS-CoV-2 pandemic, it is essential to continue to develop potent antivirals, in support of the vaccine approach.

These RNA viruses encode for proteins, forming a replication/transcription complex (RTC) that orchestrates viral replication (Ferron et al., 2017; Knipe and Howley, 2013; Ogando et al., 2019). The peculiarity of *Arenaviridae* and *Coronaviridae* families, is the unique viral 3′-5′-exoribonuclease (ExoN) activity described so far (Hastie et al., 2011; Snijder et al., 2003), The ExoN activity carried by arenavirus nucleoprotein (N) or the nsp14 protein of coronavirus participates to the suppression of the host innate immune response (Martínez-Sobrido et al., 2006, 2007, 2009; Becares et al., 2016; Lei et al., 2020), moreover the nsp14 displays an additional role in maintaining the genome integrity (Bouvet et al., 2012; Ferron et al., 2018). The arenavirus and coronavirus ExoN belonging to the same DEDD superfamily (DED/EDh subfamily), are structurally homolog (Zuo and Deutscher, 2001), and characterized by the presence of four conserved acidic residues (Asp and Glu) (Bouvet et al., 2012; Yekwa et al., 2019), essential for the binding of two metal cations (Mg^{2+} and/or Mn^{2+}) involved in the RNA hydrolysis mechanism (Steitz and Steitz, 1993), always proceeding from the 3′- to the 5′-direction.

Because of its biological significance to the viral life cycle, ExoN is an attractive target for drug-design (Papageorgiou et al., 2020; Subissi et al., 2014).

In drug development efforts using ExoN of mammarenavirus and coronavirus as targets, assays making use of radiolabeled substrate (Baddock et al., 2022; Bouvet et al., 2012; Ferron et al., 2018; Saramago et al., 2021; Yekwa et al., 2017, 2019) or mass spectrometry (Scholle et al., 2021) are available but barely adapted to HT screening. Recently, HTS assays using FRET were applied to screen SARS-CoV-2 ExoN (Canal et al., 2021; Chen et al., 2021; Rona et al., 2022).

Here we present a convenient method using fluorescence polarization (FP) to assess the ExoN activity and its inhibition. The recorded FP signal is altered proportionally to the size of the fluorescent RNA probe which is hydrolyzed into smaller fragments. We validate the method on SARS-CoV-2, Lymphocytic Choriomeningitis (LCMV) and Machupo viruses (MACV) ExoN. The method is sensitive, robust, amenable to miniaturization (384 well plates) and allowed us to screen a focused library of 113 metal chelators over the three-targeted viral ExoN, validating the proof-of-concept of the assay. We selected several hit inhibitors and determined by FP their IC_{50}. The hit compounds were tested in cellular assays.

2. Materials and methods

2.1. Products and reagents

Aurintricarboxyclic acid (**40**) was purchased from Acros Organics. Ribavirin (**82**) and Favipiravir (**83**) were purchased from Carbosynth. The library (113 compounds) containing phenyl-DKA, piperidinyl-DKA, indolyl-DKA, benzofuranyl-DKA, triazolyl-DKA (DKA families), polyphenols (POP family), *N*-hydroxyisoquinoline-1,3-diones (HID family) and miscellaneous compounds have been described previously (Saez-Ayala et al., 2018, 2019). The hit compounds **3, 4, 18, 55** and **57** have been synthesized and their synthesis will be published in due course. All compounds were resuspended in 100% DMSO at 20 mM and stored at -20 °C. The 22-mer RNA 5′-UGACGGCCCGGAAAACCGGGCC-3′ containing FAM dye at the 5′-end (5′-FAM-RNA) was purchased from Microsynth AG (Switzerland).

2.2. Protein expression and purification

All proteins were expressed in E. Coli. The LCMV and MACV ExoN plasmids used for this study were described in (Yekwa et al., 2019). For the expression of the SARS-CoV-2 nsp10 and nsp14, the synthetic genes were purchased from Twist Bioscience (USA). The protein production methods are detailed in the supplementary data file (see also Fig. S1 for elution profiles).

2.3. Set-up of exonuclease activity conditions based on fluorescent polarization assay

2.3.1. Optimization of 5′-FAM-RNA concentration, ExoN/RNA ratio, temperature, metal ion nature and concentration

Reactions were performed in 20 μl total volume in a buffer containing 40 mM Tris (pH 8), 5 mM DTT and 2 or 5 mM $MnCl_2$. For each 5′-FAM-RNA concentration (0.05, 0.1, 0.25, 0.5 and 1 μM), a range of concentration of ExoN was tested from a ratio of 5-fold less enzyme up to 10-fold more enzyme (0.01–10 μM) than 5′-FAM-RNA. For SARS-CoV-2 ExoN, the molar ratio of nsp14:nsp10 complex in the reactions was always kept at 1:4, as optimized previously (Bouvet et al., 2012) to enhance nsp14 activity.

To find the optimal temperature, metal ion nature and concentration, the 5′-FAM-RNA concentration was kept at 0.1 μM and ExoN concentration ranged from 0.1 to 1.6 μM. The activity was tested in the presence of $MnCl_2$ or $MgCl_2$ at 1, 2 or 5 mM. The FP signal was recorded either at 25 °C or at 37 °C. Negative controls tested used consisted in the replacement of $MnCl_2$ by $CaCl_2$ or, depletion of the metal ion or the enzyme. The reactions started by the addition of 5′-FAM-RNA and the fluorescence polarization (FP) was read in the Pherastar FSX (BMG

Labtech) using the 480 nm excitation and 520 nm emission filter, during 30 min at 25 °C or 37 °C, every 30 s. The gain was set up using the negative control which contained the 5′-FAM-RNA in the presence of heat-denatured nuclease. After 30 min, the reactions were stopped by the addition of an equal volume of loading buffer (8M urea containing 10 mM EDTA) and the digestion products were then loaded in 7 M urea containing 20% (wt/vol) polyacrylamide gels (acrylamide/bisacrylamide ratio 19:1) buffered with TBE and visualized using a Fluorescent Image Analyzer Typhoon (GE Healthcare).

2.3.2. Time course of ExoN assay

Reactions of 20 μl total volume were performed in the buffer mentioned above, with 2 or 5 mM $MnCl_2$ for SARS-CoV-2 or arenaviruses ExoN, respectively. The 5′-FAM-RNA concentration was fixed at 0.1 μM. The SARS-CoV-2 nsp14/nsp10 ExoN complex concentration was ranged from 0.2 to 1 μM and pre-incubation at room temperature for 5 min was performed to allow the complex formation. The LCMV and MACV ExoN concentration was ranged from 0.1 to 1.6 μM. The reaction started with the addition of 5′-FAM-RNA and The FP signal was recorded as mentioned previously. At end point, an aliquot of the sample was examined in urea PAGE as mentioned above. The assays were done in triplicate.

2.4. Screenings and IC_{50} determination

2.4.1. Screenings

The screenings at 5 μM and 20 μM inhibitor concentration were performed in 384-wells with flat bottom Nunc plates, in 20 μL total volume reaction. Reactions were performed in a buffer containing 40 mM Tris (pH 8), 5 mM DTT, with 2 or 5 mM $MnCl_2$ for SARS-CoV-2 or arenaviruses ExoN, respectively. The 5′-FAM-RNA and ExoN concentrations were fixed at 0.1 μM and 0.4 μM, respectively. Compounds (**1**–**113**) were added to the reaction with a final concentration of 5 μM and 20 μM in 5% DMSO. 8 reactions mix with ExoN were used as positive controls and 8 reactions mix with heat-denatured ExoN were used as negative controls. Reactions were initiated by adding the 5′-FAM-RNA and the FP signal was recorded as mentioned previously. To calculate the percentage of inhibition, a time correction was applied for the delayed initiation of the reaction due to the use of a multichannel pipette. The percentage of inhibition at a given time was calculated as follows:

$$inhibition\% = \frac{100 \times (FP - average\,of\,positive\,controls)}{(average\,negative\,controls - average\,positive\,controls)}$$

where FP correspond to the fluorescent polarization signal of a compound.

The time selected for doing this calculation was the time when the signal of the positive control reached the plateau (30 min). To assess the robustness of the assay we calculate the z' value.(Formula and representative scatter plot in Supplementary Fig. S3).

2.4.2. IC_{50} determination

Reactions were performed in the same experimental conditions as used for the screenings. The compound concentrations varied from 0.2 to 12.5 μM for LCMV ExoN, from 0.4 to 25 μM for MACV ExoN and from 0.5 to 16 μM for SARS-CoV-2 ExoN nsp14/nsp10 complex. The reaction started with the addition of 5′-FAM-RNA and the FP signal was recorded as mentioned previously. The percentage of inhibition was calculated as indicated in the previous section. The curves of the percentage of inhibition with respect to the inhibitor concentration in a logarithmic scale were fitted in Graphpad Prism software using a four parameters equation. The assays were done in triplicate.

2.5. Cellular assays

LCMV minigenome assays (MG) were adapted from a previously described procedure (Saez-Ayala et al., 2018, 2019). SARS-CoV-2 cellular assays were performed as previously described (Touret et al., 2020, 2021). Protocols are detailed in the supplementary data file.

3. Results and discussion

Fluorescence polarization (FP) is a reliable and sensitive tool for monitoring enzymatic reaction, by determining the difference of polarization signals (Zhang et al., 2012). FP - based assay is a robust method commonly used in drug discovery (Lea and Simeonov, 2011; Uri and Nonga, 2020). The FP signal recorded is proportional to the molecular weight (MW) of a fluorescent molecule (Kwok, 2002; Latif et al., 2001). We decided to apply this method to viral ExoN activity, by monitoring the size of a fluorescent-labeled RNA probe which is altered in the course of the nuclease, reflecting the enzymatic activity (Liu et al., 2014; Zhang et al., 2012). The assay was first optimized.

3.1. Optimization of experimental conditions of ExoN activity based on FP assay

To set-up a screening assay, we explored 5′-FAM-RNA substrate and ExoN concentration and ratio, metal ion co-factors, temperature and reaction duration. Some RNA substrate and optimal conditions were already described (Bouvet et al., 2012; Saramago et al., 2021; Yekwa et al., 2017, 2019). A 22mer RNA that forms a stable hairpin in its 3′ end has been reported to be a valuable substrate for both ExoN. Moreover, for SARS-CoV-2 ExoN, nsp10 able to stimulate nsp14 ExoN activity (Bouvet et al., 2012; Saramago et al., 2021) was added in the reaction

(ratio 1:4 of nsp14:nsp10).

We first determined the optimal 5′-FAM-RNA concentration that provides sufficient and stable FP signal, and the ratio of ExoN and 5′-FAM-RNA. For each 5′-FAM-RNA concentration (0.05–1 μM), single turnover (STO) conditions (excess of enzyme versus substrate) and also multiple turnover (MTO) conditions (excess of substrate versus enzyme) were tested. A significant change in the FP signal was observed only under STO conditions. 0.1 μM concentration of 5′-FAM-RNA was selected to provide a reproducible and stable FP signal.

To optimize the controls, several combinations were tested (Supplementary Fig. S2). For all negative controls, there was no variation between the initial and final FP values. However, we observe that the initial FP values are lower without $MnCl_2$. This result is consistent with the study of Liu et al. (2014), who reported that cations can affect the FP signal. The negative controls were then prepared by mixing 5′-FAM-RNA with $MnCl_2$ and without ExoN.

Regarding the nature of the metal ion, $MnCl_2$ and $MgCl_2$ were tested. An increased activity is observed with $MnCl_2$ (data not shown). The concentration of $MnCl_2$ that shows the highest reduction in FP signal is 5 mM for arenaviruses (Yekwa et al., 2017, 2019) and 2 mM for SARS-CoV-2 (Baddock et al., 2020; Saramago et al., 2021). Finally, the temperature of the assay is 25 °C since the incubation at 37 °C leads to a significant evaporation of the sample.

3.2. Assessing the SARS-CoV-2, LCMV and MACV ExoN activity by FP

While the 5′-FAM-RNA substrate was fixed at 0.1 μM, 0.1–1.6 μM of ExoN were tested. The FP signal was measured for 30 min. The FP curves and end point RNA degradation products examined in urea PAGE, are gathered in Fig. 1.

The negative controls (Fig. 1, brown curves, in panels A, B and C)
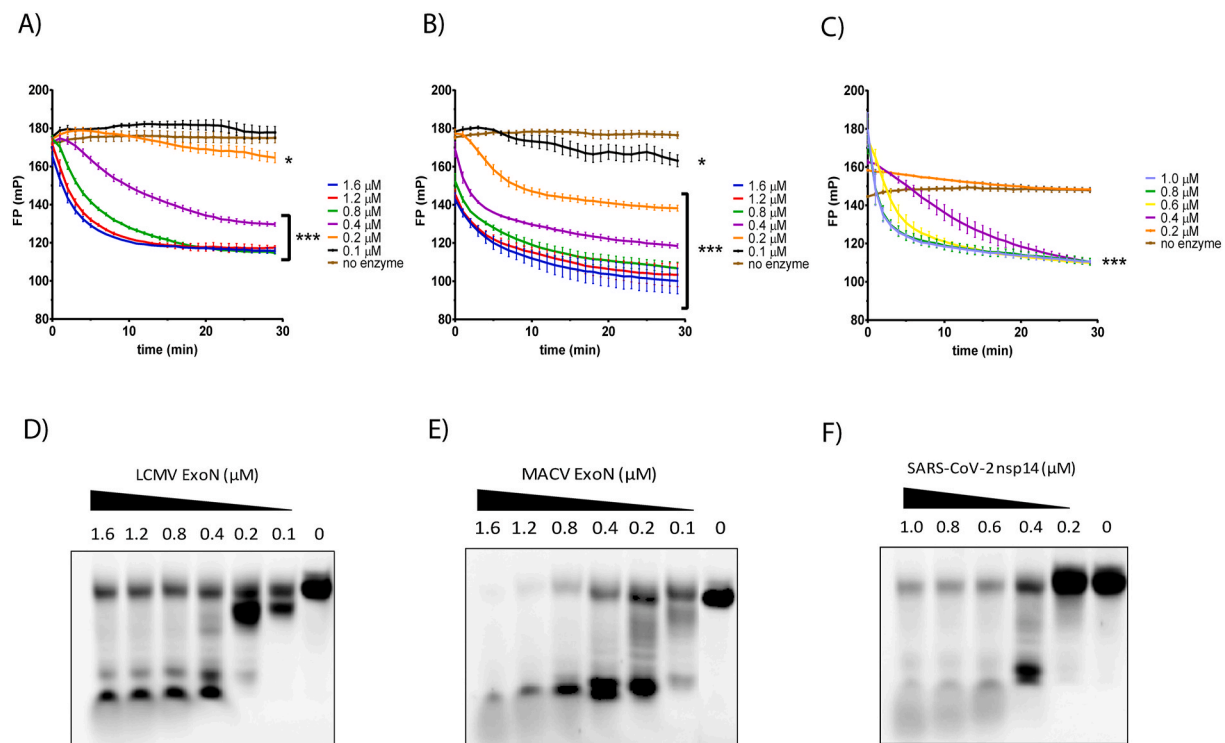
Fig. 1. ExoN activity measured by FP for LCMV (panel A), MACV (panel B) and SARS-CoV-2 (panel C). The FP signal variation is recorded with time during 30 min, each 30 secondes, at 25 °C. The 5′-FAM-RNA substrate concentration used is 0.1 μM and the ExoN concentration tested ranges 0.1 μM–1.6 μM. The data represents the average and SEM of three independent experiments. The * shows the enzyme concentrations at which the FP values are significantly different compared to the control condition (no enzyme) * p value < 0.05, *** p value < 0.001 (One-way ANOVA). The bottom panels illustrate a representative image of the digestion products analyzed in urea PAGE, of the ExoN activity for LCMV (panel D), MACV (panel E) and SARS-CoV-2 (panel F), after recording the FP signal. An aliquot of the sample was loaded into a urea-PAGE 20% and scanned in a fluorescence imager.

present flattened curves, as expected. Strikingly, a small increase in the initial FP value is observed, corresponding to the time required for the formation of the catalytic complex. This is particularly visible with SARS-CoV-2 nsp14, which requires its activation by the cofactor nsp10. Indeed, nsp14 ExoN N-terminus is flexible, when nsp10 is not bound the catalytic site of nsp14 is distorted not allowing the catalytic ions to activate the water molecule for the nucleophilic attack (Ferron et al., 2018).

For all tested ExoN, except for the lowest concentration, we observe a reduction of the FP signal with time. The decrease of the FP value is correlated with the hydrolysis of the 5′-FAM-RNA, as confirmed on the urea PAGE analysis (Fig. 1, panels D, E and F). The difference between initial and final FP value after 30 min is proportional to the number of nucleotides removed from the substrate. By increasing the ExoN concentration, we observe an increase in the FP curves slope but the FP signals reach a plateau, which might be related to the inability to remove any extra nucleotide when the RNA fragments are to shorter.

The method efficiency was validated by the difference of FP values between the negative control (Fig. 1, brown curves, in panels A, B and C) and one concentration after 30 min reaction. This difference was selected as significant enough, with ΔFP ± 30 to 60 units of mP. A molar ratio of 1:4 between the 5′-FAM-RNA (0.1 μM) and ExoN (0.4 μM) was used for the screening. The robustness of the assay was assessed by calculating the z' factor (supplementary methods and Fig. S3). For LCMV, MACV and SARS-CoV-2 we obtained z' value of 0.72, 0.74 and 0.69, respectively.

3.3. Screening of a focused library against the SARS-CoV-2, LCMV, and MACV ExoN using FP

Because ExoN activity is metal-dependent, we screened a focused library of 113 metal chelators that we have previously developed (Saez-Ayala et al., 2018, 2019), in order to demonstrate the robustness of our FP method. All compounds of the library were selected on the basis of competitive inhibition by metal chelation approach. Several patterns were chosen on the chelating scaffolds, in order to explore electronic, structural, and steric features critical for the binding process and active site accommodation. Two screenings were performed using 20 μM and 5 μM of compounds and the percentages of inhibition, deduced from FP curves, are gathered in Fig. 2 (panels A, B, and C) and in Supplementary Fig. S3, respectively.

Aurintricarboxyclic Acid (ATA, **40**), a polyphenol (POP), was included as a positive control as it has been previously described as a nuclease inhibitor (Baddock et al., 2022; Canal et al., 2021; Huang et al., 2016), acting as non-specific metal chelator (Liu et al., 2014). Compound **40** inhibits 100% of the different ExoN activity at 20 μM (Fig. 2, Table 1) and 52%, 39% and 23% at 5 μM (Supplementary Fig. S3), respectively against LCMV, MACV and SARS-CoV-2 ExoN.

We identified 5 inhibitors (**65**, **67**, **77**, **78** and **91**) of LCMV ExoN including 3 common with MACV ExoN (Fig. 2 and Table 1) with efficiency between 70 and 100% inhibition at 20 μM. Compounds **65**, **67**, **77**, **78** belong to *N*-hydroxyisoquinoline-1,3-diones (HID) family and compound **91** belongs to β-diketo acid (DKA) family were previously described by us as potent specific metal chelators (Saez-Ayala et al., 2018, 2019). 9 hit compounds (**18**, **40**, **46**, **55**, **68**, **77**, **78**, **91** and **92**) inhibiting SARS-CoV-2 ExoN with efficiency between 70 and 100% inhibition at 20 μM were also identified (Fig. 2, Table 1, Supplementary Fig. S3). Compounds **18** and **55** have never been described before. DKA **91** is the more efficient compound against all ExoN, showing inhibition at both 5 μM and 20 μM, with 87–100% inhibition at 20 μM and 37–100% inhibition at 5 μM.

3.4. IC50 measurement of hit compounds by FP

IC50 determination was performed for all hit compounds displaying more than 70% inhibition at 20 μM concentration. The dose-response
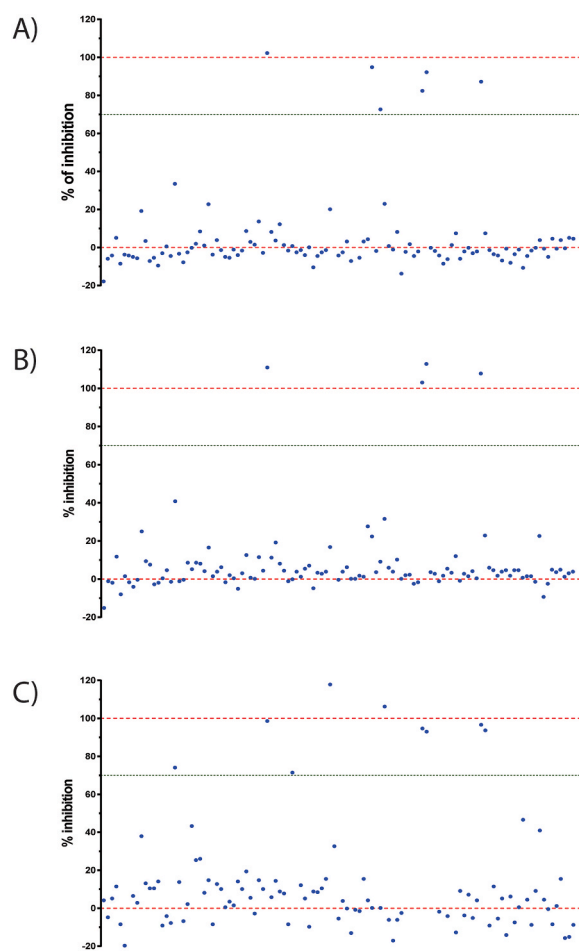
Fig. 2. Screening of focused library of metal chelators (113) against LCMV (panel A), MACV (panel B) and SARS-CoV-2 nsp14:nsp10 complex (panel C) ExoN followed by FP. The dots show the % of inhibition of the ExoN activity as described in materials and methods. For the screening conditions 0.1 μM 5′-FAM-RNA, 0.4 μM ExoN and 20 μM of inhibitor were used.

curves and IC50 values determined by hill plot curve fitting all hit compounds and reference compound **40**, are gathered in Fig. 3 and Table 1. The FP curves and the end point digestion products examined in urea PAGE are gathered in Supplementary Figs. S5–S8. IC50 determination was also performed for compounds **3**, **4**, **44** and **57** (Table 1), although they did not display high inhibition during the primary screening.

As expected, the reference compound ATA **40** was a potent inhibitor with IC50 values of 7.05 ± 0.78, 5.57 ± 0.41 and 5.50 ± 0.19 μM, for LCMV, MACV and SARS-CoV-2 ExoN, respectively. The highest inhibition observed with the DKA **91** during the two screenings was confirmed in the IC50 values. DKA **91** displayed equivalent efficiency to inhibit LCMV and MACV ExoN with respectively 5.63 ± 0.35 and 5.42 ± 0.46 μM IC50 values. The inhibition is slightly more pronounced for SARS-CoV-2 ExoN with IC50 of 1.86 ± 0.16 μM. For other hit compounds, IC50 values ranged between 6 and 24 μM. Notably, these values correlated perfectly with the inhibition % obtained by both screenings at 20 and 5 μM, confirming the robustness and reproducibility of the assay. Moreover, The FP signal correlated with the degree of digestion observed upon PAGE analysis (Supplementary Figs. S5–S8). While the HID family (compounds **65**, **67**, **68**, **77** and **78**) showed a rather broad spectrum of efficacy for both arenavirus and coronavirus ExoNs, the DKA family (phenyl-DKA, piperidinyl-DKA and triazolyl-DKA, compounds **3**, **4**, **18**, **44**, **55**, **57**, **91** and **92**) showed a clear specificity for the SARS-CoV-2 ExoN.

Table 1

List of hits compounds, targets, % of inhibition of the ExoN screening at 20 µM, ExoN- IC_{50} values, % of inhibition of the cellular screenings at 50 µM, EC_{50} and CC_{50} values and compound structures. *: monoplicate.

Cmpd N°	Target	% inhib ExoN (20 µM)	IC_{50} (µM)	% inhib Cellular Assay (50 µM)	EC_{50} (µM) CC_{50} (µM)	structure
3	SARS-CoV-2	5	>50	50	38 ± 3 >50	
4	SARS-CoV-2	11	33.8*	70	19 ± 3.7 >50	
18	SARS-CoV-2	74	20 ± 1.8	15	>50 >50	
40	LCMV	102	7.1 ± 0.8	0	ND	
	MACV	111	5.6 ± 0.4	ND	ND	
	SARS-CoV-2	99	5.5 ± 0.2	80	27 ± 20 >50	
44	SARS-CoV-2	8	>50	70	26 ± 1.7 >50	
46	SARS-CoV-2	71	12 ± 0.5	40	12 ± 3.7 >25	
55	SARS-CoV-2	118	14 ± 4	15	23 ± 3.7 >50	
57	SARS-CoV-2	−5	>50	64	8.5 ± 1.3 >50	
65	LCMV	95	16 ± 0.9	33 >50	ND	
67	LCMV	73	24 ± 0.9	39 >50	ND	
68	SARS-CoV-2	106	14.7 ± 4.6	10	>50 >50	
77	LCMV	82	16.8 ± 1.1	27	ND	
	MACV	103	13.6 ± 1.5	>50	ND	
	SARS-CoV-2	95	7.8 ± 2	ND 0	>50 >50	
78	LCMV	92	13.3 ± 1.3	31	ND	
	MACV	113	11.5 ± 0.9	>100	ND	
	SARS-CoV-2	93	6.9 ± 2	ND 0	>50 >50	
91	LCMV	87	5.6 ± 0.4	0	ND	
	MACV	108	5.4 ± 0.5	ND	ND	
	SARS-CoV-2	97	1.9 ± 0.2	0	>50 >50	
92	SARS-CoV-2	93	7.1 ± 0.5	0	>50 >50	

3.5. LCMV minigenome activity

Arenavirus replication can be modeled using a recombinant plasmid minigenome system comprising the viral RdRp (L), the nucleoprotein (N), and a LCMV genomic RNA (Ortiz-Riaño et al., 2013). Previous studies have shown the efficiency of this method (Saez-Ayala et al., 2019). We tested the hit compounds **40**, **65**, **67**, **77**, **78** and **91**, at 100 and 50 µM. Because ribavirin (**82**) is the only licensed antiviral agent with activity against arenaviruses (McCormick et al., 1986; Moreno et al., 2011), it was chosen as a reference compound. Favipiravir (**83**), having demonstrated broad-spectrum activity against a number of RNA viruses, was also added in the screening. Since the compounds were

supposed to target the polymerase function, the assay was particularly suited by measuring the GLuc reporter gene (Gluc activity %, Supplementary Fig. S9). We also tested the cytotoxic effect of the compounds at 50 and 100 µM (Cell viability %, Supplementary Fig. S9). The ribavirin (**82**) resulted in a 76% and 47% inhibition of GLuc activity, at 100 and 50 µM respectively, but was associated with important cytotoxic effect with 35 and 50% cell viability, as described previously (Mendenhall et al., 2011). Unexpectedly, favipiravir (**83**) displayed weak inhibition (30% at 100 µM) without cell viability reduction (Mendenhall et al., 2011). ATA (**40**) displayed no antiviral effect, but, cytotoxicity as described previously (Andrew et al., 1999; Haimsohn et al., 2002). Compounds **65**, **67** and **77** displayed slight effect (25–50% inhibition)
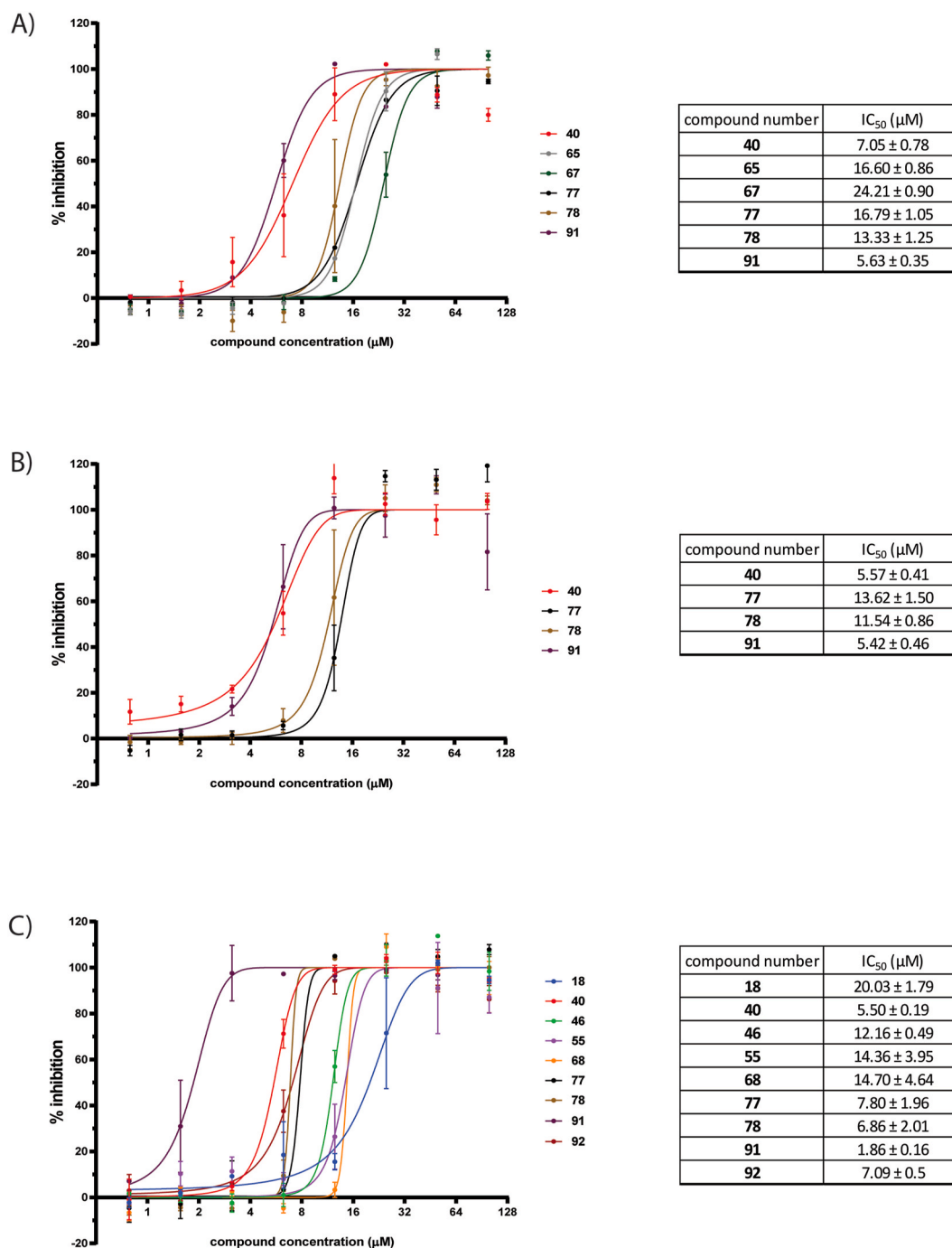
Fig. 3. IC$_{50}$ measurement of hit compounds by FP on LCMV, MACV and SARS-CoV-2 nsp14:nsp10 complex The graphs show the dose-response curves obtained by extraction of FP data and the corresponding IC$_{50}$ values for LCMV (panel A), MACV (panel B) and SARS-CoV-2 (panel C). The data represents the average and SEM of three independent experiments.

on GLuc expression but associated with cytotoxic effect, as observed for ribavirin (**82**). Compound **78** displayed weak GLuc expression inhibition (30% at 50 μM) without cytotoxicity, compared to ribavirin (**82**).

3.6. SARS-Cov-2 in vitro evaluation

The full library of 113 metal chelators was screened in a SARS-CoV-2 infected cell-based assay. We performed a primary screen for SARS-Cov-2 in VeroE6 cells (Touret et al., 2020) and we used remdesivir as a reference compound (Pruijssers et al., 2020; Wang et al., 2020). This fast and reliable assay, based on the cell viability, measures the ability of a compound to prevent the cytopathic effect induced by the viral

replication at 50 μM concentration.

Our primary screen identified 31 hit compounds that prevent cytopathic effect by at least 40% (Supplemental Fig. S10). To go further, we next performed dose-response analysis in VeroE6 TMPRSS2 (Touret et al., 2021; Weiss et al., 2021). We used VeroE6/TMPRSS2 cells to avoid off target false-positive compounds as it has been shown for Chloroquine (Hoffmann et al., 2020). Remdesivir, as reference compound, displayed EC$_{50}$ of 1.5 ± 1.1 μM with CC$_{50}$ > 10 μM.

Of the 31 primary hits, 19 compounds displaying between 40 and 100% inhibition were analyzed in dose-response assays. 7 compounds from the same family and 5 compounds displaying between 40 and 70% inhibition were set aside. Additionally, the 8 hit compounds from the

biochemical screening displaying between 0 and 40% inhibition were also analyzed. Here, we confirmed the antiviral activity of ATA (**40**) against SARS-Cov-2 in cell culture (Canal et al., 2021) with EC$_{50}$ of 27.23 ± 20.68 μM. We were unable to confirm primary efficiency of 6 potential hit compounds and we identified 5 compounds that displayed significant cytotoxicity.

Finally, we identified 4 new compounds **3**, **4**, **44**, and **57**, that displayed a robust antiviral activity with EC$_{50}$ between 8 and 38 μM without cytotoxicity and 2 compounds **46** and **55** that exert a potent antiviral activity in the same range but also showing signs of cytotoxicity, without reaching the CC$_{50}$ value (Table 1 and Supplementary Fig. S11). Compounds **46** and **55** were identified during the biochemical screening on the SARS-CoV-2 ExoN, confirming the ExoN targeting.

4. Conclusion

We proved in this study that fluorescence polarization (FP) method is reliable, sensitive to monitor nuclease activity and feasible in 384-well plates. The method is robust, rapid and non-destructive allowing the visualization of the RNA substrate degradation using gels as orthogonal method of confirmation. We identified several hit inhibitors of viral arenavirus (LCMV and MACV) and coronavirus (SARS-CoV-2) ExoN activity and determined by fluorescence polarization their IC$_{50}$ at a micromolar level. Then we validated their activities in cell culture assays and we found compounds displaying efficiency at micromolar level against SARS-CoV-2. These results highlight the effectiveness of fluorescence polarization assay in the screening of compounds libraries for the discovery of antivirals.

Appendix A. Supplementary data

Supplementary data to this article can be found online at https://doi.org/10.1016/j.antiviral.2022.105364.

References

Andrew, D.J., Hay, A.W., Evans, S.W., 1999. Aurintricarboxylic acid inhibits apoptosis and supports proliferation in a haemopoietic growth-factor dependent myeloid cell line. Immunopharmacology 41, 1–10. https://doi.org/10.1016/s0162-3109(98)00049-6.

Baddock, H.T., Brolih, S., Yosaatmadja, Y., Ratnaweera, M., Bielinski, M., Swift, L.P., Cruz-Migoni, A., Fan, H., Keown, J.R., Walker, A.P., Morris, G.M., Grimes, J.M., Fodor, E., Schofield, C.J., Gileadi, O., McHugh, P.J., 2022. Characterization of the SARS-CoV-2 ExoN (nsp14ExoN-nsp10) complex: implications for its role in viral genome stability and inhibitor identification. Nucleic Acids Res. 50, 1484–1500. https://doi.org/10.1093/nar/gkab1303.

Baddock, H.T., Brolih, S., Yosaatmadja, Y., Ratnaweera, M., Bielinski, M., Swift, L.P., Cruz-Migoni, A., Morris, G.M., Schofield, C.J., Gileadi, O., McHugh, P.J., 2020. Characterisation of the SARS-CoV-2 ExoN (nsp14ExoN-nsp10) complex: implications

for its role in viral genome stability and inhibitor identification. bioRxiv. https://doi.org/10.1101/2020.08.13.248211, 2020.08.13.248211.

Becares, M., Pascual-Iglesias, A., Nogales, A., Sola, I., Enjuanes, L., Zuñiga, S., 2016. Mutagenesis of coronavirus nsp14 reveals its potential role in modulation of the innate immune response. J. Virol. 90, 5399–5414. https://doi.org/10.1128/JVI.03259-15.

Bouvet, M., Imbert, I., Subissi, L., Gluais, L., Canard, B., Decroly, E., 2012. RNA 3'-end mismatch excision by the severe acute respiratory syndrome coronavirus nonstructural protein nsp10/nsp14 exoribonuclease complex. Proc. Natl. Acad. Sci. USA 109, 9372–9377. https://doi.org/10.1073/pnas.1201130109.

Canal, B., McClure, A.W., Curran, J.F., Wu, M., Ulferts, R., Weissmann, F., Zeng, J., Bertolin, A.P., Milligan, J.C., Basu, S., Drury, L.S., Deegan, T.D., Fujisawa, R., Roberts, E.L., Basier, C., Labib, K., Beale, R., Howell, M., Diffley, J.F.X., 2021. Identifying SARS-CoV-2 antiviral compounds by screening for small molecule inhibitors of nsp14/nsp10 exoribonuclease. Biochem. J. 478, 2445–2464. https://doi.org/10.1042/BCJ20210198.

Chen, T., Fei, C.-Y., Chen, Y.-P., Sargsyan, K., Chang, C.-P., Yuan, H.S., Lim, C., 2021. Synergistic inhibition of SARS-CoV-2 replication using disulfiram/Ebselen and remdesivir. ACS Pharmacol. Transl. Sci. 4, 898–907. https://doi.org/10.1021/acsptsci.1c00022.

Ferron, F., Subissi, L., Silveira De Morais, A.T., Le, N.T.T., Sevajol, M., Gluais, L., Decroly, E., Vonrhein, C., Bricogne, G., Canard, B., Imbert, I., 2018. Structural and molecular basis of mismatch correction and ribavirin excision from coronavirus RNA. Proc. Natl. Acad. Sci. U.S.A. 115, E162–E171. https://doi.org/10.1073/pnas.1718806115.

Ferron, F., Weber, F., de la Torre, J.C., Reguera, J., 2017. Transcription and replication mechanisms of Bunyaviridae and Arenaviridae L proteins. Virus Res. 234, 118–134. https://doi.org/10.1016/j.virusres.2017.01.018.

Haimsohn, M., Beery, R., Karasik, A., Kanety, H., Geier, A., 2002. Aurintricarboxylic acid induces a distinct activation of the IGF-I receptor signaling within MDA-231 cells. Endocrinology 143, 837–845. https://doi.org/10.1210/endo.143.3.8681.

Hastie, K.M., Kimberlin, C.R., Zandonatti, M.A., MacRae, I.J., Saphire, E.O., 2011. Structure of the Lassa virus nucleoprotein reveals a dsRNA-specific 3′ to 5′ exonuclease activity essential for immune suppression. Proc. Natl. Acad. Sci. U.S.A. 108, 2396–2401. https://doi.org/10.1073/pnas.1016404108.

Hoffmann, M., Mösbauer, K., Hofmann-Winkler, H., Kaul, A., Kleine-Weber, H., Krüger, N., Gassen, N.C., Müller, M.A., Drosten, C., Pöhlmann, S., 2020. Chloroquine does not inhibit infection of human lung cells with SARS-CoV-2. Nature 585, 588–590. https://doi.org/10.1038/s41586-020-2575-3.

Huang, K.-W., Hsu, K.-C., Chu, L.-Y., Yang, J.-M., Yuan, H.S., Hsiao, Y.-Y., 2016. Identification of inhibitors for the DEDDh family of exonucleases and a unique inhibition mechanism by crystal structure analysis of CRN-4 bound with 2-Morpholin-4-ylethanesulfonate (MES). J. Med. Chem. 59, 8019–8029. https://doi.org/10.1021/acs.jmedchem.6b00794.

Knipe, D.M., Howley, P.M. (Eds.), 2013. Fields Virology, sixth ed. Wolters Kluwer/Lippincott Williams & Wilkins Health, Philadelphia, PA.

Kwok, P.-Y., 2002. SNP genotyping with fluorescence polarization detection. Hum. Mutat. 19, 315–323. https://doi.org/10.1002/humu.10058.

Latif, S., Bauer-Sardina, I., Ranade, K., Livak, K.J., Kwok, P.Y., 2001. Fluorescence polarization in homogeneous nucleic acid analysis II: 5'-nuclease assay. Genome Res. 11, 436–440. https://doi.org/10.1101/gr.156601.

Lea, W.A., Simeonov, A., 2011. Fluorescence polarization assays in small molecule screening. Expet Opin. Drug Discov. 6, 17–32. https://doi.org/10.1517/17460441.2011.537322.

Lei, X., Dong, X., Ma, R., Wang, W., Xiao, X., Tian, Z., Wang, C., Wang, Y., Li, L., Ren, L., Guo, F., Zhao, Z., Zhou, Z., Xiang, Z., Wang, J., 2020. Activation and evasion of type I interferon responses by SARS-CoV-2. Nat. Commun. 11, 3810. https://doi.org/10.1038/s41467-020-17665-9.

Liu, X., Chen, Y., Fierke, C.A., 2014. A real-time fluorescence polarization activity assay to screen for inhibitors of bacterial ribonuclease P. Nucleic Acids Res. 42, e159. https://doi.org/10.1093/nar/gku850.

Martínez-Sobrido, L., Emonet, S., Giannakas, P., Cubitt, B., García-Sastre, A., de la Torre, J.C., 2009. Identification of amino acid residues critical for the anti-interferon activity of the nucleoprotein of the prototypic arenavirus lymphocytic choriomeningitis virus. J. Virol. 83, 11330–11340. https://doi.org/10.1128/JVI.00763-09.

Martínez-Sobrido, L., Giannakas, P., Cubitt, B., García-Sastre, A., de la Torre, J.C., 2007. Differential inhibition of type I interferon induction by arenavirus nucleoproteins. J. Virol. 81, 12696–12703. https://doi.org/10.1128/JVI.00882-07.

Martínez-Sobrido, L., Zúñiga, E.I., Rosario, D., García-Sastre, A., de la Torre, J.C., 2006. Inhibition of the type I interferon response by the nucleoprotein of the prototypic arenavirus lymphocytic choriomeningitis virus. J. Virol. 80, 9192–9199. https://doi.org/10.1128/JVI.00555-06.

McCormick, J.B., King, I.J., Webb, P.A., Scribner, C.L., Craven, R.B., Johnson, K.M., Elliott, L.H., Belmont-Williams, R., 1986. Lassa fever. Effective therapy with ribavirin. N. Engl. J. Med. 314, 20–26. https://doi.org/10.1056/NEJM198601023140104.

Mendenhall, M., Russell, A., Juelich, T., Messina, E.L., Smee, D.F., Freiberg, A.N., Holbrook, M.R., Furuta, Y., de la Torre, J.-C., Nunberg, J.H., Gowen, B.B., 2011. T-705 (favipiravir) inhibition of arenavirus replication in cell culture. Antimicrob. Agents Chemother. 55, 782–787. https://doi.org/10.1128/AAC.01219-10.

Moreno, H., Gallego, I., Sevilla, N., de la Torre, J.C., Domingo, E., Martín, V., 2011. Ribavirin can Be mutagenic for arenaviruses. J. Virol. 85, 7246–7255. https://doi.org/10.1128/JVI.00614-11.

Ogando, N.S., Ferron, F., Decroly, E., Canard, B., Posthuma, C.C., Snijder, E.J., 2019. The curious case of the nidovirus exoribonuclease: its role in RNA synthesis and

replication fidelity. Front. Microbiol. 10, 1813. https://doi.org/10.3389/fmicb.2019.01813.

Ortiz-Riaño, E., Cheng, B.Y.H., Carlos de la Torre, J., Martínez-Sobrido, L., 2013. Arenavirus reverse genetics for vaccine development. J. Gen. Virol. 94, 1175–1188. https://doi.org/10.1099/vir.0.051102-0.

Papageorgiou, N., Spiliopoulou, M., Nguyen, T.-H.V., Vaitsopoulou, A., Laban, E.Y., Alvarez, K., Margiolaki, I., Canard, B., Ferron, F., 2020. Brothers in arms: structure, assembly and function of Arenaviridae nucleoprotein. Viruses 12. https://doi.org/10.3390/v12070772.

Pruijssers, A.J., George, A.S., Schäfer, A., Leist, S.R., Gralinksi, L.E., Dinnon, K.H., Yount, B.L., Agostini, M.L., Stevens, L.J., Chappell, J.D., Lu, X., Hughes, T.M., Gully, K., Martinez, D.R., Brown, A.J., Graham, R.L., Perry, J.K., Du Pont, V., Pitts, J., Ma, B., Babusis, D., Murakami, E., Feng, J.Y., Bilello, J.P., Porter, D.P., Cihlar, T., Baric, R.S., Denison, M.R., Sheahan, T.P., 2020. Remdesivir inhibits SARS-CoV-2 in human lung cells and chimeric SARS-CoV expressing the SARS-CoV-2 RNA polymerase in mice. Cell Rep. 32, 107940 https://doi.org/10.1016/j.celrep.2020.107940.

Rona, G., Zeke, A., Miwatani-Minter, B., de Vries, M., Kaur, R., Schinlever, A., Garcia, S. F., Goldberg, H.V., Wang, H., Hinds, T.R., Bailly, F., Zheng, N., Cotelle, P., Desmaële, D., Landau, N.R., Dittmann, M., Pagano, M., 2022. The NSP14/NSP10 RNA repair complex as a Pan-coronavirus therapeutic target. Cell Death Differ. 29, 285–292. https://doi.org/10.1038/s41418-021-00900-1.

Saez-Ayala, M., Laban Yekwa, E., Mondielli, C., Roux, L., Hernández, S., Bailly, F., Cotelle, P., Rogolino, D., Canard, B., Ferron, F., Alvarez, K., 2019. Metal chelators for the inhibition of the lymphocytic choriomeningitis virus endonuclease domain. Antivir. Res. 162, 79–89. https://doi.org/10.1016/j.antiviral.2018.12.008.

Saez-Ayala, M., Yekwa, E.L., Carcelli, M., Canard, B., Alvarez, K., Ferron, F., 2018. Crystal structures of Lymphocytic choriomeningitis virus endonuclease domain complexed with diketo-acid ligands. IUCrJ 5, 223–235. https://doi.org/10.1107/S2052252518001021.

Saramago, M., Bárria, C., Costa, V., Souza, C.S., Viegas, S.C., Domingues, S., Lousa, D., Soares, C.M., Arraiano, C.M., Matos, R.G., 2021. New targets for drug design: importance of nsp14/nsp10 complex formation for the 3'-5' exoribonucleolytic activity on SARS-CoV-2. bioRxiv, 425745. https://doi.org/10.1101/2021.01.07.425745, 2021.01.07.

Scholle, M.D., Liu, C., Deval, J., Gurard-Levin, Z.A., 2021. Label-free screening of SARS-CoV-2 NSP14 exonuclease activity using SAMDI mass spectrometry. SLAS Discov. Adv. Life Sci. R D 26, 766–774. https://doi.org/10.1177/24725552211008854.

Snijder, E.J., Bredenbeek, P.J., Dobbe, J.C., Thiel, V., Ziebuhr, J., Poon, L.L.M., Guan, Y., Rozanov, M., Spaan, W.J.M., Gorbalenya, A.E., 2003. Unique and conserved features of genome and proteome of SARS-coronavirus, an early split-off from the coronavirus group 2 lineage. J. Mol. Biol. 331, 991–1004. https://doi.org/10.1016/S0022-2836(03)00865-9.

Steitz, T.A., Steitz, J.A., 1993. A general two-metal-ion mechanism for catalytic RNA. Proc. Natl. Acad. Sci. U.S.A. 90, 6498–6502. https://doi.org/10.1073/pnas.90.14.6498.

Subissi, L., Imbert, I., Ferron, F., Collet, A., Coutard, B., Decroly, E., Canard, B., 2014. SARS-CoV ORF1b-encoded nonstructural proteins 12-16: replicative enzymes as antiviral targets. Antivir. Res. 101, 122–130. https://doi.org/10.1016/j.antiviral.2013.11.006.

Touret, F., Driouich, J.-S., Cochin, M., Petit, P.R., Gilles, M., Barthélémy, K., Moreau, G., Mahon, F.-X., Malvy, D., Solas, C., de Lamballerie, X., Nougairède, A., 2021. Preclinical evaluation of Imatinib does not support its use as an antiviral drug against SARS-CoV-2. Antivir. Res. 193, 105137 https://doi.org/10.1016/j.antiviral.2021.105137.

Touret, F., Gilles, M., Barral, K., Nougairède, A., van Helden, J., Decroly, E., de Lamballerie, X., Coutard, B., 2020. In vitro screening of a FDA approved chemical library reveals potential inhibitors of SARS-CoV-2 replication. Sci. Rep. 10, 13093 https://doi.org/10.1038/s41598-020-70143-6.

Uri, A., Nonga, O.E., 2020. What is the current value of fluorescence polarization assays in small molecule screening? Expet Opin. Drug Discov. 15, 131–133. https://doi.org/10.1080/17460441.2020.1702966.

Wang, M., Cao, R., Zhang, L., Yang, X., Liu, J., Xu, M., Shi, Z., Hu, Z., Zhong, W., Xiao, G., 2020. Remdesivir and chloroquine effectively inhibit the recently emerged novel coronavirus (2019-nCoV) in vitro. Cell Res. 30, 269–271. https://doi.org/10.1038/s41422-020-0282-0.

Weiss, A., Touret, F., Baronti, C., Gilles, M., Hoen, B., Nougairède, A., Lamballerie, X. de, Sommer, M.O.A., 2021. Niclosamide shows strong antiviral activity in a human airway model of SARS-CoV-2 infection and a conserved potency against the Alpha (B.1.1.7), Beta (B.1.351) and Delta variant (B.1.617.2). PLoS One 16, e0260958. https://doi.org/10.1371/journal.pone.0260958.

Yekwa, E., Aphibanthammakit, C., Carnec, X., Picard, C., Canard, B., Baize, S., Ferron, F., 2019. Arenaviridae exoribonuclease presents genomic RNA edition capacity. bioRxiv 541698. https://doi.org/10.1101/541698.

Yekwa, E., Khourieh, J., Canard, B., Papageorgiou, N., Ferron, F., 2017. Activity inhibition and crystal polymorphism induced by active-site metal swapping. Acta Crystallogr. Sect. Struct. Biol. 73, 641–649. https://doi.org/10.1107/S205979831700866X.

Zhang, M., Le, H.-N., Wang, P., Ye, B.-C., 2012. A versatile molecular beacon-like probe for multiplexed detection based on fluorescence polarization and its application for a resettable logic gate. Chem. Commun. Camb. Engl. 48, 10004–10006. https://doi.org/10.1039/c2cc35185d.

Zuo, Y., Deutscher, M.P., 2001. Exoribonuclease superfamilies: structural analysis and phylogenetic distribution. Nucleic Acids Res. 29, 1017–1026.